DOI: 10.1002/cphc.201100030

Multi-Field Effect on the Electronic Properties of Silicon Nanowires

Ren Qin Zhang, Chao Hou, Nan Gao, Zi Wen,* and Qing Jiang*[a]

The quantum confinement and electronic properties of silicon nanowires (SiNWs) under an external strain field ε and an electric field **E**—as well as both (ε plus **E**)—are systematically investigated using density functional theory. These two fields exist in working environments of integrated circuits. It is found that both ε and **E** lead to a drop of the band gap $E_g(\varepsilon,\mathbf{E})$ of the SiNWs. If both fields coexist, the interaction between ε and **E** causes that $E_g(\varepsilon,\mathbf{E})$ becomes orientation-dependent, which results from variations of both the conduction-band minimum and the valence-band maximum. The interaction is further illustrated by the density of states near the Fermi level and the eigenvalue of the highest occupied molecular orbital.

1. Introduction

Since bulk quantities of silicon nanowires (SiNWs) were first prepared by using a technique that combines laser ablation and vapor–liquid–solid growth,[1] these materials have attracted great interest because of their interface compatibility with the present silicon-based technology and the need to achieve high integration in very-large-scale integration circuits.[2,3] They are building blocks of silicon-based nanodevices because they can function both as devices and as wires that access them.[4] It has been possible to fabricate SiNWs with controllable sizes and morphologies by using various techniques;[5–9] this allows SiNWs to have wide applications in field-effect transistors (FETs),[10,11] photodetectors,[12] sensors,[13,14] field-emission devices,[15] photovoltaic cells[16] and logic gates,[17,18] especially in device miniaturization.[2,4,19] In these applications of SiNWs, external fields, such as a strain field ε or an electric field **E**, are ubiquitous. Understanding the influence of these external fields on the electronic band structures of SiNWs is an important element in integrating SiNWs into nanodevices. To design and optimize SiNW-based nanodevices, it is important to gain physical understanding of the effects of these fields on the electronic band structures of the SiNWs from a fundamental point of view.

The parameter ε can be used as an excellent band-engineering strategy for the design of semiconductor devices. Homles et al. experimentally demonstrated that ε can modulate the optical properties of SiNWs, where the strain-induced photoluminescence of the SiNWs has a wide energy range.[20,21] In silicon-based devices, ε (as a design element) improves the mobility of the electrons[19] and enhances the transconductance in FETs.[22] By using first principle calculations, it was found that ε can tune the electronic properties of [100],[23–25] [110],[23,24,26] [111],[23,26,27] and [112][28,29] SiNWs, and can cause changes in the valence- and conduction-band edge states, leading to a transition between indirect and direct band gaps.[23–29] This parameter also affects the carrier effective masses of the SiNWs,[24,26,27] which determine the mobility behaviors of those wires. In addition, partial strain in SiNWs induces a charge separation where electrons and holes are located at different ends of the nanowires. This opens up a new avenue for designing solar cells by morphology control.[30]

The effect of **E**, being similar to that of ε, can induce a band-gap deformation of the semiconductors.[31] **E** leads to an overlapping of the valence and conduction bands of monocrystalline graphitic films with a strong ambipolar electronic field effect.[32] **E** can also help manipulate Si nanomaterials to fabricate new types of electronic devices[33] and manipulate the growth of SiNWs.[34] Since **E** is easy to control in actual applications, it should be a powerful tool to modulate the electronic band structures of SiNWs. In electronic nanodevices, the presence of **E** is required and the field affects the electrical and structural properties of the SiNWs.[31] Increasing **E** at an SiNW–SiO_2 interface enhances the performance of nanoscale memory cells.[35] Practically, SiNWs on an insulating substrate can be subjected to a strong **E** through an applied gate voltage. Such systems are prototype nanoscale FETs. In addition, the combined effect of ε and **E** affects the properties of SiNWs as well. It has been reported that the band gap $E_g(\varepsilon,\mathbf{E})$ of carbon nanotubes can be affected by various combinations of ε and **E**.[36,37]

High-performance SiNW-based nanodevices require an accurate control of the properties of the SiNWs at the atomic level. This requirement could be easily realized with the help of computer simulations while experimental measurements are difficult to perform. Band calculations are at the foundation of understanding the electronic properties of semiconductor materials. Therefore, herein, density functional theory (DFT) is used to study the band structures of SiNWs under external fields. The results not only enhance our understanding of the effect of

[a] R. Q. Zhang, C. Hou, N. Gao, Prof. Z. Wen, Prof. Q. Jiang
Key Laboratory of Automobile Materials (Jilin University)
Ministry of Education, and School of Materials Science
and Engineering, Jilin University, Changchun, 130022 (China)
Fax: (+86) 431-85095876
E-mail: wenzi@jlu.edu.cn
jiangq@jlu.edu.cn

 WILEY ONLINE LIBRARY © 2011 Wiley-VCH Verlag GmbH & Co. KGaA, Weinheim

the external fields, but also have guiding significance for applications of SiNWs.

Computational Details and Methods

The structures of the SiNWs calculated herein are shown in Figure 1. The starting structure was obtained from bulk Si. The dangling bonds of the surface Si atoms for the SiNWs were terminated by H at an initial bond length of 0.154 nm. The growth direction of the SiNWs was along the Z axis, with periodicity. Although the X and Y directions have periodicity too, there was a vacuum space at least 12 Å outside the considered SiNW structures, which ensures that the structures are one-dimensional; this vacuum space was large enough to eliminate any influence of the SiNWs on the neighboring cells. The cross-sections of the [100], [110], [111], and [112] SiNWs were regular tetragon, hexagon, regular hexagon, and tetragon, respectively. In accordance with experimental observations[5,6,38] and the Wulff construction,[39] the SiNWs had low free-energy facets of (111), (110), and (100). [100] and [111] SiNWs were enclosed with (110) facets, while [110] SiNWs were bound with (100) and (111) facets, and that of the [112] SiNWs were (110) and (111) facets, as displayed in Figure 1.

The calculations were carried out by using DFT,[40,41] which is provided in the DMol3 program code.[42,43] The generalized gradient approximation (GGA) functional with the HCTH method,[44] which is nonlocal functional, was used as the exchange-correlation (XC) functional. The all-electron relativitistic (AER) procedure,[45] which includes all core electrons explicitly and introduces some relativistic effects into the core, was used for the core treatments. In addition, double numerical plus polarization (DNP)[42] was chosen as the basis set with an orbital cutoff of 4.6 Å. We used smearing techniques[46] with a smearing value of 0.005 Ha (1 Ha = 27.2114 eV). The structure of the SiNWs was then relaxed using the delocalized internal coordinate optimization scheme. Monkhorst–Pack sampling with $1\times1\times5$, $1\times1\times6$, $1\times1\times3$, and $1\times1\times4$ k-point grids was used for the structural optimizations of the [100], [110], [111], and [112] SiNWs, respectively. We also tested higher k-point grids, the results of band gaps were found to be the same as those obtained using the above k-point grids. The convergence energy tolerance was 1.0×10^{-5} Ha, the maximum force was 0.002 Ha Å^{-1}, and the maximum displacement was 0.005 Å in the geometry optimization.

HCTH is a well-chosen functional, unlike the PW91 functional,[47] giving accurate $E_g(D)$ values of both bulk Si and hydrogen-terminated SiNWs. The pair of electrons with opposite spins occupies one orbital without dangling bond, whereby the material properties are mostly determined by the correlation part. The HCTH functional with an accurate correlation part has improved XC potentials,[44,48,49] which leads to accurate $E_g(D)$ values. Using the HCTH functional, the values $a_0 = 5.474$ Å and $E_g(\infty) = 1.24$ eV were determined, which only differ from the experimental results of 5.431 Å[50] and 1.17 eV[51] by 0.79% and 5.98%, respectively. The $E_g(D)$ value of the [112] SiNWs calculated by the HCTH functional in our simulations were in good agreement with the experimental results[5] and the calculated results obtained using the hybrid functional Hamiltonian (HFH),[52] as shown in Figure 2. It was found that the PW91 functional underestimates the $E_g(D)$ values whereas the HCTH functional leads to more accurate ones. Taking the E_g(2.5 nm) of the [112] SiNWs as an example, we found that E_g(2.5 nm) = 1.74 eV was obtained using the HCTH functional, which corresponds to the HFH result of 1.72 eV and the experimental result of 1.6 eV within an error of 1.16% and 8.75%, respectively. In addition, we compared the E_g(3.0 nm) = 1.48 eV of the [110] SiNWs calculated using the HCTH functional with the experimental

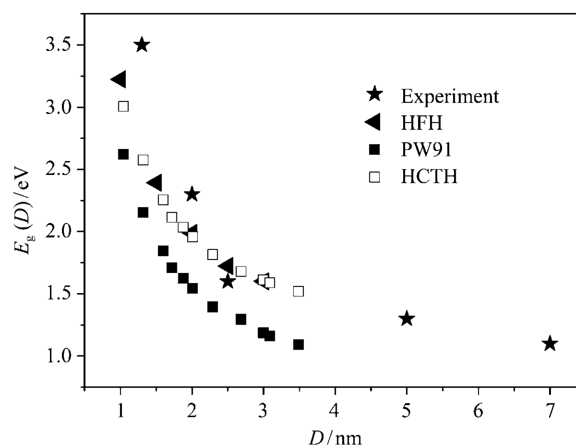

Figure 2. Calculated $E_g(D)$ of [112] SiNWs with the PW91 (■) and HCTH (□) functionals as a function of D. The results calculated with the HFH functional (triangles) and experimental results (★) are given for comparison purpose.

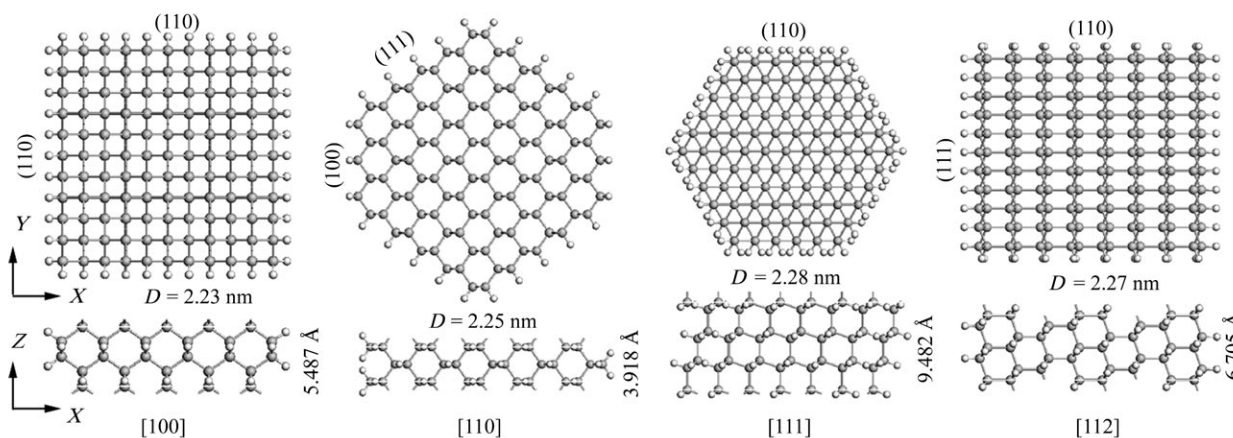

Figure 1. Top and side views of the ball and stick structures of H-terminated [100], [110], [111], and [112] SiNWs where the enclosed surfaces indexes are given. The big and small balls denote Si and H atoms, respectively. The diameter D the of SiNWs is defined as the diameter of a circle with the same area. The lengths of the repeating units of SiNWs along the Z axis and the D values are shown.

 © 2011 Wiley-VCH Verlag GmbH & Co. KGaA, Weinheim

result of 1.50 eV,[5] observing an error of 1.3 %. Note that for the smallest D, our results are lower than the experimental results, due to unknown reasons.

An ε was applied by changing the unit-cell size along the growth direction. The coordinates of all the atoms were relaxed to obtain their equilibrium positions without any constraints, except for the cell sizes. $\varepsilon = \pm 0 \sim 10\%$ in 1 % increments wass added axially, since the elastic limit of SiNWs with $D < 10$ nm was about 0.1 ± 0.02.[53] The positive and negative values of ε represent tensile and compressive strains, respectively. **E** is directly added along the radial direction with strengths of $\mathbf{E} = 0$, 5, 10, 15, 20, 25, 30 MV cm^{-1}, respectively. A multi-field is realized by applying ε and **E** simultaneously. Note that since the D of the SiNWs is in the nanometer range, considering the largest diameter in our study of 2.27 nm, we only need 4.54 V to reach a field intensity of 20 MV cm^{-1}. Thus, the application of our results of electric field is practical. In the presence of **E**, the Hamiltonian H is composed of the potential arising from **E**, the kinetic operator T, and the Hartree (V_H), and exchange-correlation (V_{XC}) potential, that is, $H = T + V_H + V_{XC} - e\mathbf{E}$. It is argued that the application of **E** in a periodic direction is not trivial.[54] However, in our calculations, **E** was applied along the radial direction, where there is large enough vacuum to ensure that the term is linear in real space for the corresponding potential of the system. As firstly discussed by Neugebauer et al.,[55] when **E** is applied in a periodic system, an artifact electric field is observed which is a result of the forced periodicity. This artifact has an effect on the total energy[56] and the resulting dipole,[57] thus inducing erroneous results. To verify that our vacuum space was large enough to avoid this effect, we increased this space from 12 to 16 Å with increments of 2 Å. Taking the [100] SiNWs as an example (under $\mathbf{E} = 30$ MV cm^{-1}), we obtained the calculated total energy, the resulting dipole and the E_g listed in Table 1. The dipoles were calculated by the Hirshfeld method.[58] It was found that the total energy, the resulting dipole, and the band gap were insensitive to the vacuum space within an error range of 1 %, implying that the results well converge with vacuum of 12 Å.

Table 1. The total energy, the resulting dipole and E_g of [100] SiNWs vary with different vacuum spaces under $\mathbf{E} = 30$ MV cm^{-1}.[a]

Vacuum space [Å]	Total energy [Ha]	Dipole [a.u.]	E_g [eV]
12	−29031.9529439	0.1174	0.728
14	−29031.9526068	0.1171	0.732
16	−29031.9523745	0.1169	0.734

[a] Note that after carefully checking the dipoles of all the atoms, we found that there is almost no variation. Therefore, only the dipoles of a surface Si atom are listed in this table.

Although the surface chemistry has a strong effect on the band structure of the SiNWs, depending on the saturation groups and the coverage,[59–61] we excluded such factors and concentrated on the effect of external fields on the electronic properties of SiNWs saturated with H. For all the SiNWs, we carefully checked the H saturation from the Si–H bond length and the electron transfer from the Si atoms under the external fields. Both with and without external fields, the Si–H bond length is around 1.50 Å, which is almost identical to that of the SiH_4 cluster (1.49 Å). From an analysis of the total number of electrons in saturated H, there is little electron transfer from the Si to the H atoms with or without external fields. The terminated H atoms do not introduce additional energy bands at the band edges because the binding energy of the H–Si bond is larger than that of the Si–Si bond. The band edges are determined by core Si–Si bonds. We thus affirm that variations in the electronic band structures of the SiNWs under external fields are not related to saturated H.

2. Results and Discussion

Figure 3 shows $E_g(D)$ functions for [100], [110], [111], and [112] SiNWs where $1.0 < D < 4.7$ nm. As D decreases, $E_g(D)$ increases due to the quantum-confinement effect.[5,62–64] $E_g(D)$ should

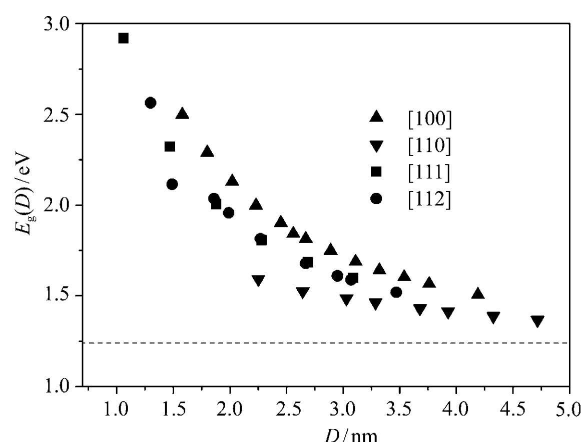

Figure 3. Calculated $E_g(D)$ of [100] (▲), [110] (▼), [111] (■), and [112] (●) SiNWs as a function of D. The dashed line (-----) denotes the calculated $E_g(\infty)$ value for reference.

slowly decrease and gradually approache $E_g(\infty) = 1.24$ eV as $D > 5$ nm. $E_g(D)$ is orientation-dependent[65,66] on an order of $E_g^{100}(D) > E_g^{111}(D) \approx E_g^{112}(D) > E_g^{110}(D)$. We can understand this anisotropy of $E_g(D)$ through the binding energy E_b of the Si–Si bond in the SiNWs. We calculated the E_b values of the Si–Si bond in [100], [110], [111], and [112] SiNWs, which have the stoichiometry $Si_{100}H_{40}$, $Si_{80}H_{28}$, $Si_{182}H_{66}$, and $Si_{126}H_{46}$ in each unit cell, respectively. Using E_b^{110} as a reference, the energy differences of E_b^{100}, E_b^{111} and E_b^{112} were found to be 53, 25 and 28 meV, respectively, or $E_b^{100} > E_b^{111} \approx E_b^{112} > E_b^{110}$, having the same series for the anisotropy of $E_g(D)$ as that given above.

Electronic band-structure modulations with ε are strongly dependent on the crystal orientations and the diameters of the SiNWs.[23,26,30] Herein, we discuss the results obtained for [100], [110], [111], and [112] SiNWs, as shown in Figure 4. The facet distances along the axial direction of the SiNWs are different. Therefore, ε can affect the electronic band structures of the SiNWs in different ways. Variations of the conduction-band minimum (CBM) and the valence-band maximum (VBM) under ε, combined with their location in the k-space, determine the change of $E_g(\varepsilon)$. CBM and VBM values located at the same and different k-points result in direct and indirect band gaps, respectively.

For the [100] SiNWs, the negative ε firstly increases and then decreases $E_g(\varepsilon)$ as ε changes from −2% to −10% while the positive ε causes a monotonous decrease of $E_g(\varepsilon)$, as presented

 © 2011 Wiley-VCH Verlag GmbH & Co. KGaA, Weinheim

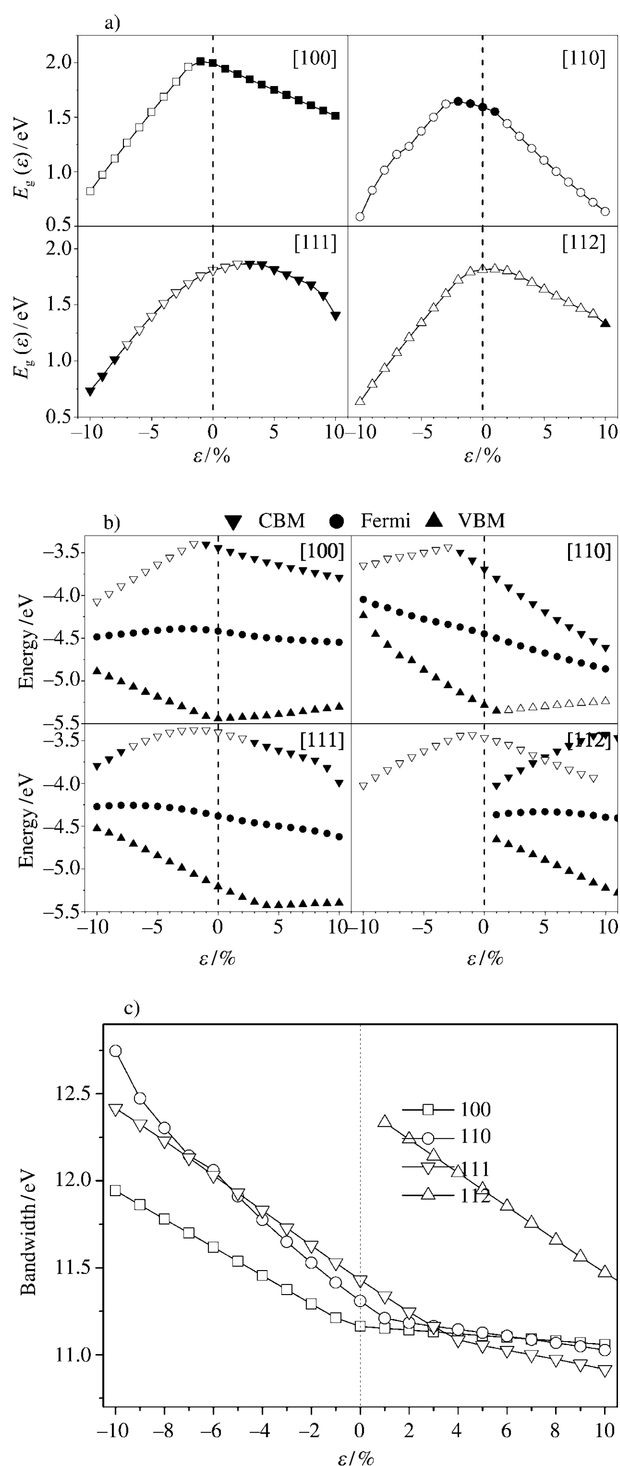

Figure 4. a) $E_g(\varepsilon)$, b) E_{CBM}, Fermi level, and E_{VBM}, and c) valence band width as a function of ε for [100] ($Si_{100}H_{40}$), [110] ($Si_{80}H_{28}$), [111] ($Si_{182}H_{66}$), and [112] ($Si_{126}H_{46}$) SiNWs. In (a), the filled and empty symbols denote the direct and indirect band gaps, respectively. In (b), the filled and empty symbols represent locating and non-locating at the Γ-point in the *k*-space, respectively. The reference potential is the vacuum level. The dashed (-----) line denotes the situation of $\varepsilon=0$.

in Figure 4a. The direct-to-indirect transition of $E_g(\varepsilon)$ occurs at $\varepsilon=-2\%$ due to the location change of CBM, as shown in Figure 4b . E_{VBM} increases with both types of strains, while negative ε has a larger effect. This variation is determined by the change of the valence bandwidth, as shown in Figure 4c. It was found that the bandwidth monotonously increases as the negative ε increases while it is almost insensitive to the positive ε. For variations of E_{CBM}, the positive ε leads to a monotonous drop whereas the negative ε first causes it to increase (until $\varepsilon=-2\%$) and then to decrease.

For the [110] SiNWs, the negative ε has a similar effect on $E_g(\varepsilon)$ as that observed for the [100] SiNWs and induces a direct-to-indirect transition under $\varepsilon=-3\%$. Although the positive ε causes a monotonous decrease of $E_g(\varepsilon)$, a direct-to-indirect transition occurs under $\varepsilon=2\%$. In contrast to the transition under a negative ε, a positive ε causes the location of the VBM to migrate from the Γ-point, which results in a direct-to-indirect transition, as shown in Figure 4b. These results are consistent with that reported by Wu et al.[30] Further, the variation of the valence bandwidth with ε is analyzed and shown in Figure 4c. A negative ε changes the valence bandwidth more pronouncedly than a positive ε, which results in the larger variation of the VBM under a negative ε.

Contrary to the [100] and [110] SiNWs, for the [111] SiNWs, $E_g(\varepsilon)$ decreases monotonously under a negative ε while a positive ε increases $E_g(\varepsilon)$ until $\varepsilon=4\%$, and then causes it to decrease. An indirect-to-direct transition occurs under $\varepsilon=-7\%$ and $\varepsilon=3\%$. For the [112] SiNWs, both negative and positive ε decrease $E_g(\varepsilon)$ while an indirect-to-direct transition occurs

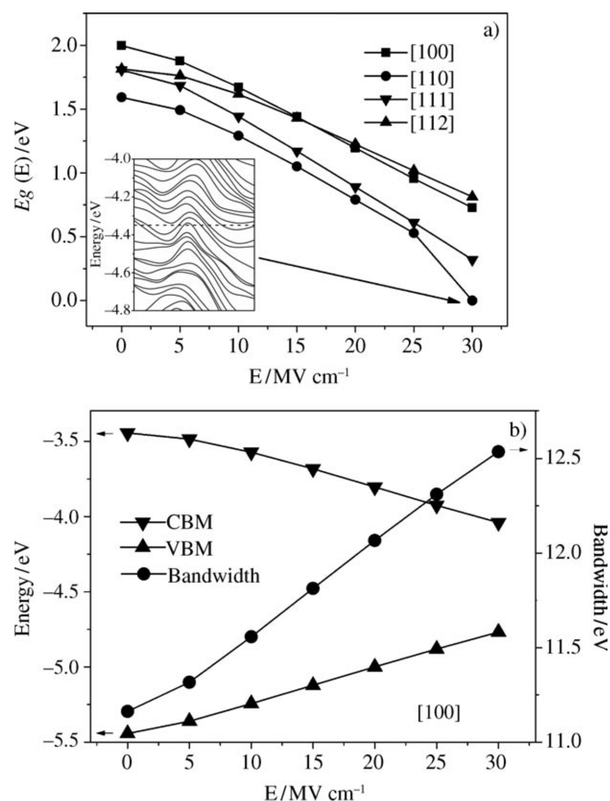

Figure 5. a) E_g(**E**) as function of **E** for [100] ($Si_{100}H_{40}$), [110] ($Si_{80}H_{28}$), [111] ($Si_{182}H_{66}$), and [112] ($Si_{126}H_{46}$) SiNWs. The inset shows the electronic band structure around the Fermi level (-----) of the [110] SiNWs under **E** $=30$ MV cm^{-}, where the bands crossing the Fermi level result in $E_g(30)=0$. b) E_{CBM}, E_{VBM}, and valence bandwidth of [100] SiNWs as a function of **E**. The reference potential is the vacuum level.

under $\varepsilon = 10\%$. The discrepancy with the referenced results comes from the different crossing section of the [112] SiNWs, which confirms that the crossing section is an important factor for application of [112] SiNWs with a direct band gap.[28,29] In addition, the Fermi energy decreases with increasing ε from -10% to 10%. ε has the largest effect on the Fermi level of [110] SiNWs among the considered systems. This determines the variations of the work function, which increases with increasing ε, with ε having the largest effect on that of the [110] SiNWs.[26]

A decrease in E_g can also be achieved if **E** is applied along the radial direction of the SiNWs. Figure 5a presents the $E_g(\mathbf{E})$ function for SiNWs. **E** reduces $E_g(\mathbf{E})$, being similar to the case under an axial electric field.[31] For the [110] SiNWs, $E_g(\mathbf{E})$ is closed at $\mathbf{E} = 30$ MV cm^{-1}, that is, a semiconductor–metal transition (SMT) occurs, which is confirmed from the electronic band structure in the inset of Figure 5a. It is reported that an SMT—and even an insulator–metal transition—could occur under **E**.[67]

$E_g(\mathbf{E})$ drops are related to changes in E_{CBM} and E_{VBM}. Because of the similar situations observed for SiNWs with different orientations, our discussion will concentrate on the [100] SiNWs. As shown in Figure 5b, E_{CBM} decreases and E_{VBM} increases under **E**. The variation amounts are the same and $E_g(\mathbf{E})$ decreases. Also, the bandwidth of the valence band is related to the bond lengths and the overlap between the orbitals increases as **E** increases, which leads to an approach between the CBM and the VBM. Note that the conduction bands exhibit the same size change.

The evolution of $E_g(\varepsilon,\mathbf{E})$ as a function of ε under $\mathbf{E} = 0$, 10, 20 MV cm^{-1} are given in Figure 6. As a whole, the evolutional trend of $E_g(\varepsilon,\mathbf{E})$ is similar to the case under different **E**. At a given ε, the $E_g(\varepsilon,\mathbf{E})$ of the SiNWs decreases with increasing **E**. However, the drop rates are ε-dependent. Considering the [100] SiNWs, as ε increases, $E_g(\varepsilon,\mathbf{E})$ increases until a maximum at $\varepsilon = -2\%$. Then, $E_g(\varepsilon,\mathbf{E})$ drops. Similar to the behavior of $E_g(\varepsilon,0)$, a positive ε monotonously reduces $E_g(\varepsilon,\mathbf{E})$. Compared with $E_g(\varepsilon,0)$, $dE_g(\varepsilon,\mathbf{E})/d\varepsilon$ becomes small under a negative ε while it is almost constant under a positive ε when $\mathbf{E} = 10$, 20 MV cm^{-1}. Thus, an interaction between ε and **E** is present. To understand this interaction, we define $E_g^1 = E_g(\varepsilon,0) - [E_g(0,0) - E_g(0,10)]$ and $E_g^2 = E_g(\varepsilon,0) - [E_g(0,0) - E_g(0,20)]$, which denote simple additions of the effects of ε and $\mathbf{E} = 10$, 20 MV cm^{-1} on $E_g(\varepsilon,\mathbf{E})$, that is, $dE_g^1/d\varepsilon = dE_g^2/d\varepsilon = dE_g(\varepsilon,0)/d\varepsilon$. As shown in Figure 6a, for the [100] SiNWs, $E_g^1 < E_g(\varepsilon,10)$ and $E_g^2 < E_g(\varepsilon,20)$ when $\varepsilon < 0$, while $E_g^1 = E_g(\varepsilon,10)$ and $E_g^2 = E_g(\varepsilon,20)$ if $\varepsilon > 0$. The results show that **E** weakens the drop effect of a negative ε on $E_g(\varepsilon,\mathbf{E})$ and there is no interac-

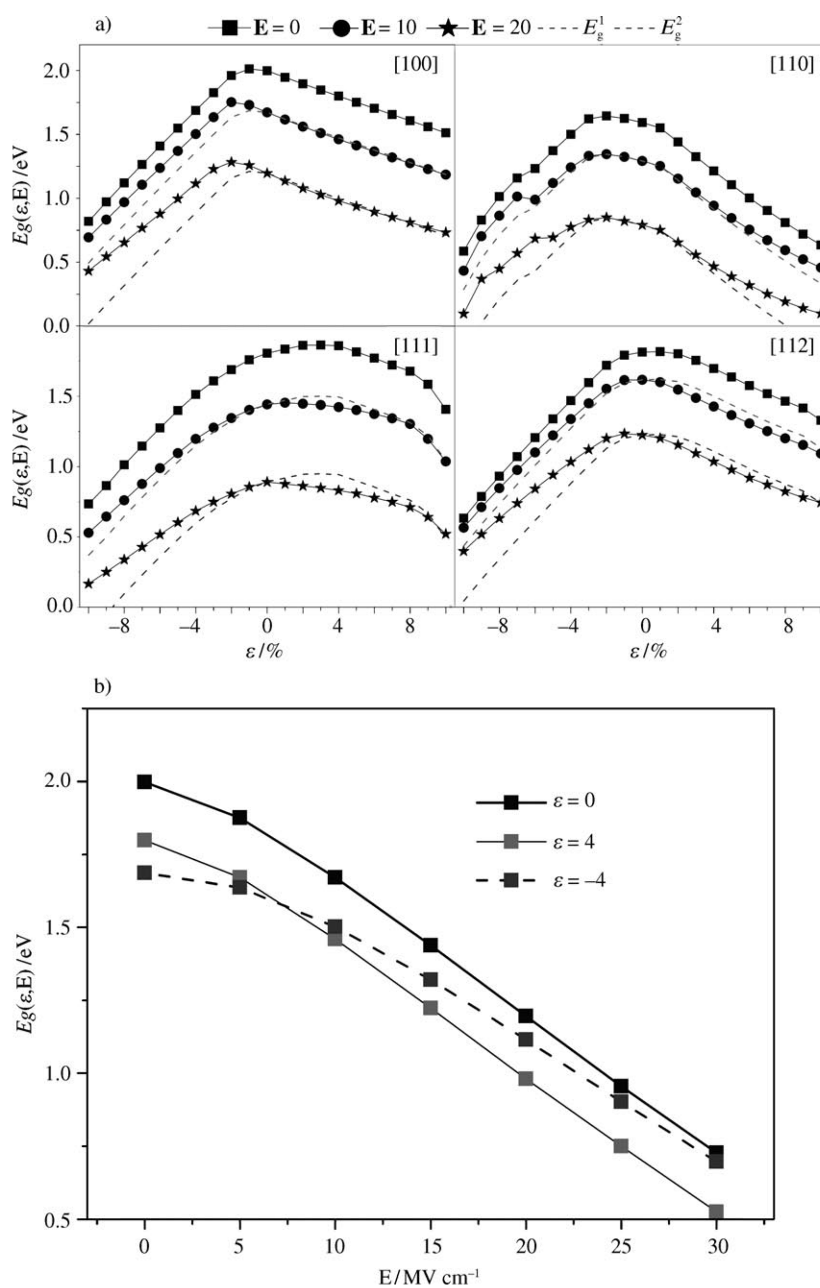

Figure 6. a) $E_g(\varepsilon,\mathbf{E})$ as a function of ε ($-10\% \leq \varepsilon \leq 10\%$ with 1% increment) under **E** ($\mathbf{E} = 0$, 10, and 20 MV cm^{-1}) for [100] ($Si_{100}H_{40}$), [110] ($Si_{80}H_{28}$), [111] ($Si_{182}H_{66}$), and [112] ($Si_{126}H_{46}$) SiNWs. The legend is shown at the top. b) $E_g(\varepsilon,\mathbf{E})$ as a function of **E** under $\varepsilon = 0$ and $\pm 4\%$ for [100] SiNWs.

 © 2011 Wiley-VCH Verlag GmbH & Co. KGaA, Weinheim

tion between a positive ε and $\mathbf{E}$ on $E_g(\varepsilon,\mathbf{E})$. It is also found that a bigger $\mathbf{E}$ enhances the interaction because of $dE_g(\varepsilon,10)/d\varepsilon > dE_g(\varepsilon,20)/d\varepsilon$.

For the [110] SiNWs, in the range of $-2\% \leq \varepsilon \leq 2\%$, the interaction between ε and $\mathbf{E}$ is small. When $\varepsilon > 3\%$, the drop effect of ε on $E_g(\varepsilon,\mathbf{E})$ is weakened by $\mathbf{E}$. For the [111] and [112] SiNWs, $\mathbf{E}$ weakens the dropping effect of the negative ε on $E_g(\varepsilon,\mathbf{E})$ while it enhances that of the positive ε. However, when $\varepsilon \rightarrow 10\%$, the interaction is weak. Similar to the case of the [100] SiNWs, a bigger $\mathbf{E}$ enhances the interaction between ε and $\mathbf{E}$ in the $E_g(\varepsilon,\mathbf{E})$ of the [110], [111], and [112] SiNWs. The interaction is also orientation-dependent, as shown in Figure 6a. To further elucidate the interaction between ε and $\mathbf{E}$, taking the [100] SiNWs as an example, we show the $E_g(\varepsilon,\mathbf{E})$ for the [100] SiNWs at $\varepsilon = \pm 4\%$ as a function of $\mathbf{E}$ in Figure 6b. $dE_g(-4,\mathbf{E})/d\mathbf{E} < dE_g(0,\mathbf{E})/d\mathbf{E} = dE_g(4,\mathbf{E})/d\mathbf{E}$. In view of the influence of ε on $\mathbf{E}$, a negative ε weakens the decreasing effect of $\mathbf{E}$ on $E_g(\varepsilon,\mathbf{E})$.

Figure 7 shows $E_{CBM}(\varepsilon,10)$ and $E_{VBM}(\varepsilon,10)$ functions. Similar to the above discussion for E_g^1, we define $E_{ref}^{CBM}(\varepsilon, 10) = E_{CBM}(\varepsilon,0) - [E_{CBM}(0,0) - E_{CBM}(0,10)]$ and $E_{ref}^{VBM}(\varepsilon, 10) = E_{VBM}(\varepsilon,0) - [E_{VBM}(0,0) - E_{VBM}(0,10)]$ as a simple addition of E_{CBM} and E_{VBM} for SiNWs, respectively. Considering [100] SiNWs under a negative ε, $E_{ref}^{CBM}(\varepsilon, 10) < E_{CBM}(\varepsilon,10)$ and $E_{ref}^{VBM}(\varepsilon, 10) > E_{VBM}(\varepsilon,10)$ result in a weakened drop effect of ε at $\mathbf{E} = 10$ MV cm^{-1}. However, the difference between $E_{ref}^{CBM}(\varepsilon, 10)$ and $E_{CBM}(\varepsilon,10)$ is smaller than that between $E_{ref}^{VBM}(\varepsilon, 10)$ and $E_{VBM}(\varepsilon,0)$, which means that the interaction effect between ε and $\mathbf{E}$ on $E_{VBM}(\varepsilon,\mathbf{E})$ mainly contributes to the interaction on $E_g(\varepsilon,\mathbf{E})$. When $\varepsilon > 0$, as shown in Figure 7, the interaction effects on $E_{CBM}(\varepsilon,10)$ and $E_{VBM}(\varepsilon,0)$ are small since $E_{ref}^{CBM}(\varepsilon, 10) = E_{CBM}(\varepsilon,10)$ and $E_{ref}^{VBM}(\varepsilon, 10) = E_{VBM}(\varepsilon,10)$.

For the [110] SiNWs, the interaction between a negative ε and $\mathbf{E}$ at $E_{CBM}(\varepsilon,\mathbf{E})$ is responsible for the changes in $E_g(\varepsilon,\mathbf{E})$ whereas that between a positive ε and $\mathbf{E}$ at both $E_{CBM}(\varepsilon,\mathbf{E})$ and $E_{VBM}(\varepsilon,\mathbf{E})$ contributes almost equally to $E_g(\varepsilon,\mathbf{E})$. For the [111] and [112] SiNWs, we observe almost the same situation, namely, that the interaction between ε and $\mathbf{E}$ on $E_{VBM}(\varepsilon,\mathbf{E})$ weakens the dropping effect on $E_g(\varepsilon,\mathbf{E})$ with a negative ε and enhances it with a positive ε.

Figure 8 presents the density of states (DOS) of [100] SiNWs under ε, $\mathbf{E}$. Under $\varepsilon = -4\%$, combined with Figure 4b, ε affects both the conduction- and the valence-band edges. Under $\mathbf{E} = 10$ MV cm^{-1}, although the valence-band edge shifts less than that solely under $\varepsilon = -4\%$, one small peak appears in the band edge with splitting of states. When $\varepsilon = -4\%$ and $\mathbf{E} = 10$ MV cm^{-1}, the peak becomes stronger, due to interaction effects between ε and $\mathbf{E}$. This demonstrates that the interaction mainly influences $E_{VBM}(\varepsilon,\mathbf{E})$.

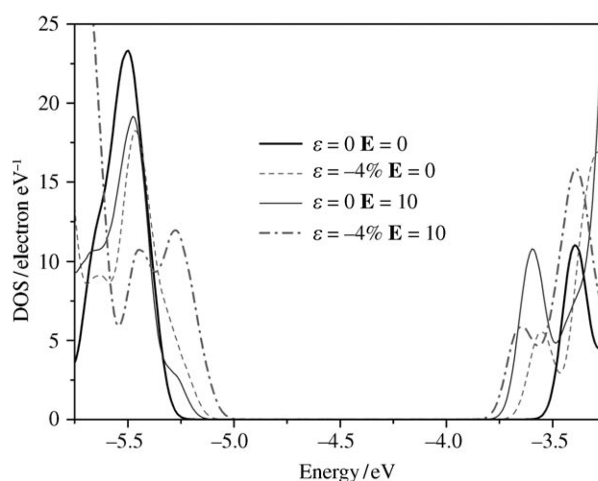

Figure 8. DOS of [100] SiNWs under $\varepsilon = -4\%$, $\mathbf{E} = 10$ MV cm^{-1}, and $\varepsilon = -4\%$ plus $\mathbf{E} = 10$ MV cm^{-1}, compared with that in the absence of external fields. The reference potential is the vacuum level.

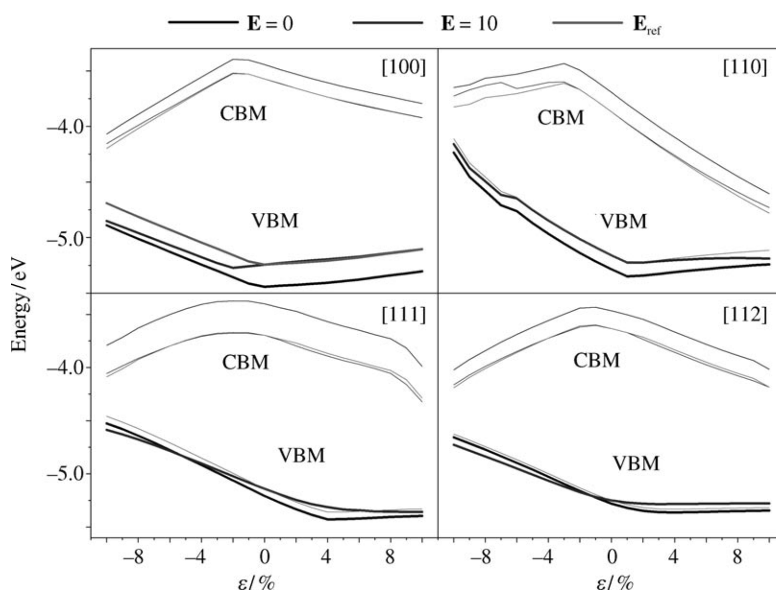

Figure 7. Evolution of E_{CBM} and E_{VBM} as a function of ε under $\mathbf{E} = 0$, 10 MV cm^{-1} for [100], [110], [111], and [112] SiNWs. The reference potential is the vacuum level.

Finally, taking the [100] SiNWs as an example, we analyze the eigenvalue of the highest occupied molecular orbital (HOMO), $E_{HOMO}(\varepsilon,\mathbf{E})$, where the distribution of HOMO corresponds to the wavefunctions of the VBM at the Γ-point, which is useful to understand how the effects of the ε and $\mathbf{E}$ fields combine. We know that a negative ε decreases the distance between nodal surfaces perpendicular to the wire axis, which results in an increased E_{VBM}.[30] For the [100] SiNWs, $E_{HOMO}(-4,0) - E_{HOMO}(0,0) = 0.23$ eV and $E_{HOMO}(-4,10) - E_{HOMO}(0,10) = 0.09$ eV. The latter is smaller than the former. Thus, $\mathbf{E}$ weakens the dropping effect of a negative ε. This result can also be applied to other SiNWs.

 © 2011 Wiley-VCH Verlag GmbH & Co. KGaA, Weinheim

We believe that our results could have important implications regarding SiNW performance in the presence of a multifield, as well as SiNW integrations in electronic devices. The combination of the advantages of the ε and **E** effects is excellent to modulate the band gap of SiNWs in order to satisfy the need of nanodevices. Simultaneously, these results help us understand how the properties of SiNWs subjected to an external field may influence the performance of electronic nanodevices.

3. Conclusions

In summary, the effects of external fields on the electronic band structures of H-terminated [100], [110], [111], and [112] SiNWs have been studied by DFT calculations using HCTH as the XC functional. Due to the quantum-confinement effect, $E_g(D)$ increases with smaller D values of the SiNWs. Both ε and **E** can cause $E_g(\varepsilon,\mathbf{E})$ to drop while it changes fascinatingly under multi-fields due to the interaction between ε and **E**, which is reported for the first time. **E** could weaken or enhance the effect of ε on variations of $E_g(\varepsilon,\mathbf{E})$, whereby the interaction is orientation-dependent. By presenting variations of E_{CBM} and E_{VBM} under multi-fields, we have provided an explanation on how the interaction influences $E_g(\varepsilon,\mathbf{E})$. From an analysis of the DOS, we found that ε changes the splitting of states induced by **E**, which leads to interactions between the ε and **E** effects. The combination of ε and **E** may provide additional flexibility and reduce the need for very large ε and **E** values to modulate the properties of SiNWs.

Acknowledgements

We acknowledge support by the National Key Basic Research Development Program (Grant No. 2010CB631001) and the Program for Changjiang Scholars and Innovative Research Team in University, and thank the High Performance Computing Center (HPCC) of Jilin University for supercomputer time.

Keywords: density functional calculations · electronic properties · electronic structure · nanomaterials · silicon

[1] A. M. Morales, C. M. Lieber, *Science* **1998**, *279*, 208 – 211.
[2] P. S. Peercy, *Nature* **2000**, *406*, 1023 – 1026.
[3] R. Rurali, *Rev. Mod. Phys.* **2010**, *82*, 427.
[4] P. Zhang, T. S. Mayer, T. N. Jackson, *ACS Nano* **2007**, *1*, 6 – 9.
[5] D. D. D. Ma, C. S. Lee, F. C. K. Au, S. Y. Tong, S. T. Lee, *Science* **2003**, *299*, 1874 – 1877.
[6] Y. Wu, Y. Cui, L. Huynh, C. J. Barrelet, D. C. Bell, C. M. Lieber, *Nano Lett.* **2004**, *4*, 433 – 436.
[7] Y. Wang, K. K. Lew, T. T. Ho, L. Pan, S. W. Novak, E. C. Dickey, J. M. Redwing, T. S. Mayer, *Nano Lett.* **2005**, *5*, 2139 – 2143.
[8] Y. Shan, S. J. Fonash, *ACS Nano* **2008**, *2*, 429 – 434.
[9] R.-Q. Zhang, Y. Lifshitz, S. T. Lee, *Adv. Mater.* **2003**, *15*, 635 – 640.
[10] Y. Cui, C. M. Lieber, *Science* **2001**, *291*, 851 – 853.
[11] J. Goldberger, A. I. Hochbaum, R. Fan, P. Yang, *Nano Lett.* **2006**, *6*, 973 – 977.
[12] C. Yang, C. J. Barrelet, F. Capasso, C. M. Lieber, *Nano Lett.* **2006**, *6*, 2929 – 2934.
[13] A. Cattani-Scholz, D. Pedone, M. Dubey, S. Neppl, B. Nickel, P. Feulner, J. Schwartz, G. Abstreiter, M. Tornow, *ACS Nano* **2008**, *2*, 1653 – 1660.
[14] G.-J. Zhang, G. Zhang, J. H. Chua, R.-E. Chee, E. H. Wong, A. Agarwal, K. D. Buddharaju, N. Singh, Z. Gao, N. Balasubramanian, *Nano Lett.* **2008**, *8*, 1066 – 1070.
[15] J. C. She, S. Z. Deng, N. S. Xu, R. H. Yao, J. Chen, *Appl. Phys. Lett.* **2006**, *88*, 013112 – 013113.
[16] K. Peng, X. Wang, S.-T. Lee, *Appl. Phys. Lett.* **2008**, *92*, 163103 – 163103.
[17] Y. Huang, X. F. Duan, Y. Cui, L. J. Lauhon, K. H. Kim, C. M. Lieber, *Science* **2001**, *294*, 1313 – 1317.
[18] B. A. Sheriff, D. Wang, J. R. Heath, J. N. Kurtin, *ACS Nano* **2008**, *2*, 1789 – 1798.
[19] M. Ieong, B. Doris, J. Kedzierski, K. Rim, M. Yang, *Science* **2004**, *306*, 2057 – 2060.
[20] D. M. Lyons, K. M. Ryan, M. A. Morris, J. D. Holmes, *Nano Lett.* **2002**, *2*, 811 – 816.
[21] G. Audoit, E. N. Mhuircheartaigh, S. M. Lipson, M. A. Morris, W. J. Blau, J. D. Holmes, *J. Mater. Chem.* **2005**, *15*, 4809 – 4815.
[22] A. Seike, T. Tange, Y. Sugiura, I. Tsuchida, H. Ohta, T. Watanabe, D. Kosemura, A. Ogura, I. Ohdomari, *Appl. Phys. Lett.* **2007**, *91*, 202117 – 202113.
[23] K.-H. Hong, J. Kim, S.-H. Lee, J. K. Shin, *Nano Lett.* **2008**, *8*, 1335 – 1340.
[24] D. Shiri, Y. Kong, A. Buin, M. P. Anantram, *Appl. Phys. Lett.* **2008**, *93*, 073114 – 073113.
[25] R. N. Sajjad, K. Alam, *J. Appl. Phys.* **2009**, *105*, 044307 – 044306.
[26] P. W. Leu, A. Svizhenko, K. Cho, *Phys. Rev. B* **2008**, *77*, 235 305 – 235 314.
[27] G. W. Peng, Y. P. Feng, *Appl. Phys. Lett.* **2007**, *91*, 083116 – 083113.
[28] A. J. Lu, R. Q. Zhang, S. T. Lee, *Appl. Phys. Lett.* **2007**, *91*, 263107 – 263103.
[29] L. Huang, N. Lu, J.-A. Yan, M. Y. Chou, C.-Z. Wang, K.-M. Ho, *J. Phys. Chem. C* **2008**, *112*, 15680 – 15683.
[30] Z. Wu, J. B. Neaton, J. C. Grossman, *Nano Lett.* **2009**, *9*, 2418 – 2422.
[31] R. Q. Zhang, W. T. Zheng, Q. Jiang, *J. Phys. Chem. C* **2009**, *113*, 10384 – 10389.
[32] K. S. Novoselov, A. K. Geim, S. V. Morozov, D. Jiang, Y. Zhang, S. V. Dubonos, I. V. Grigorieva, A. A. Firsov, *Science* **2004**, *306*, 666 – 669.
[33] I.-W. Lyo, P. Avouris, *Science* **1991**, *253*, 173 – 176.
[34] O. Englander, D. Christensen, J. Kim, L. Lin, S. J. S. Morris, *Nano Lett.* **2005**, *5*, 705 – 708.
[35] J. Fu, N. Singh, K. D. Buddharaju, S. H. G. Teo, C. Shen, Y. Jiang, C. X. Zhu, M. B. Yu, G. Q. Lo, N. Balasubramanian, D. L. Kwong, E. Gnani, G. Baccarani, *IEEE Electron Device Lett.* **2008**, *29*, 518 – 521.
[36] Y. Guo, W. Guo, *J. Phys. D* **2003**, *36*, 805 – 811.
[37] Y. V. Shtogun, L. M. Woods, *J. Phys. Chem. C* **2009**, *113*, 4792 – 4796.
[38] C.-P. Li, C. S. Lee, X. L. Ma, N. Wang, R. Q. Zhang, S. T. Lee, *Adv. Mater.* **2003**, *15*, 607 – 609.
[39] S. Hong, M. Y. Chou, *Phys. Rev. B* **1998**, *57*, 6262.
[40] P. Hohenberg, W. Kohn, *Phys. Rev.* **1964**, *136*, B864.
[41] W. Kohn, L. J. Sham, *Phys. Rev.* **1965**, *140*, A1133.
[42] B. Delley, *J. Chem. Phys.* **1990**, *92*, 508 – 517.
[43] B. Delley, *J. Chem. Phys.* **2000**, *113*, 7756 – 7764.
[44] A. D. Boese, N. C. Handy, *J. Chem. Phys.* **2001**, *114*, 5497 – 5503.
[45] D. D. Koelling, B. N. Harmon, *J. Phys. C* **1977**, *10*, 3107 – 3114.
[46] B. Delley in *Theoretical and Computational Chemistry, Vol. 2* (Eds.: J. M. Seminario, P. Politzer), Elsevier, **1995**, pp. 221 – 254.
[47] J. P. Perdew, Y. Wang, *Phys. Rev. B* **1992**, *45*, 13244.
[48] P. P. Rushton, S. J. Clark, D. J. Tozer, *Phys. Rev. B* **2001**, *63*, 115 206.
[49] L.-H. Li, L. Chen, J.-Q. Li, L.-M. Wu, *J. Phys. Chem. C* **2009**, *113*, 15384 – 15389.
[50] C. R. Hubbard, H. E. Swanson, F. A. Mauer, *J. Appl. Crystallogr.* **1975**, *8*, 45 – 48.
[51] N. W. Ashcroft, N. D. Mermin, *Solid State Physics* (Ed.: D. Garbose Crane), Harcourt Brase College Publisher, Philadelphia, **1976**.
[52] R. Rurali, B. Aradi, T. Frauenheim, A. Gali, *Phys. Rev. B* **2007**, *76*, 113 303 – 113 304.
[53] T. Kizuka, Y. Takatani, K. Asaka, R. Yoshizaki, *Phys. Rev. B* **2005**, *72*, 035 333 – 035 336.
[54] X. Wang, D. Vanderbilt, *Phys. Rev. B* **2007**, *75*, 115 116.
[55] J. Neugebauer, M. Scheffler, *Phys. Rev. B* **1992**, *46*, 16067.
[56] L. Bengtsson, *Phys. Rev. B* **1999**, *59*, 12301.
[57] A. Natan, L. Kronik, Y. Shapira, *Appl. Surf. Sci.* **2006**, *252*, 7608 – 7613.
[58] B. Delley, *Chem. Phys.* **1986**, *110*, 329 – 338.
[59] P. W. Leu, B. Shan, K. Cho, *Phys. Rev. B* **2006**, *73*, 195 320 – 195 325.

 © 2011 Wiley-VCH Verlag GmbH & Co. KGaA, Weinheim

[60] M. Nolan, S. O'Callaghan, G. Fagas, J. C. Greer, T. Frauenheim, *Nano Lett.* **2007**, *7*, 34–38.
[61] X. Blase, M. V. Fernandez-Serra, *Phys. Rev. Lett.* **2008**, *100*, 046802–046804.
[62] M. Li, J. C. Li, *Mater. Lett.* **2006**, *60*, 2526–2529.
[63] B. Delley, E. F. Steigmeier, *Appl. Phys. Lett.* **1995**, *67*, 2370–2372.
[64] X. Zhao, C. M. Wei, L. Yang, M. Y. Chou, *Phys. Rev. Lett.* **2004**, *92*, 236805.
[65] R. Q. Zhang, Y. Lifshitz, D. D. D. Ma, Y. L. Zhao, T. Frauenheim, S. T. Lee, S. Y. Tong, *J. Chem. Phys.* **2005**, *123*, 144703–144705.
[66] M.-F. Ng, L. Zhou, S.-W. Yang, L. Y. Sim, V. B. C. Tan, P. Wu, *Phys. Rev. B* **2007**, *76*, 155435.
[67] D. Zhang, G. Guo, C. Liu, R. Q. Zhang, *J. Phys. Chem. B* **2006**, *110*, 23633–23636.

Received: January 13, 2011
Revised: March 4, 2011

© 2011 Wiley-VCH Verlag GmbH & Co. KGaA, Weinheim